HOKKAIDO UNIVERSITY

Title	Excited-State Relaxation of Hydrated Thymine and Thymidine Measured by Liquid-Jet Photoelectron Spectroscopy: Experiment and Simulation
Author(s)	Buchner, Franziska; Nakayama, Akira; Yamazaki, Shohei; Ritze, Hans-Hermann; Luebcke, Andrea
Citation	Journal of the American Chemical Society, 137(8), 2931-2938 https://doi.org/10.1021/ja511108u
Issue Date	2015-03-05
Doc URL	http://hdl.handle.net/2115/58853
Rights(URL)	http://creativecommons.org/licenses/by/4.0/
Type	article
File Information	ja511108u.pdf

Instructions for use

Hokkaido University Collection of Scholarly and Academic Papers : HUSCAP

This is an open access article published under a Creative Commons Attribution (CC-BY) License, which permits unrestricted use, distribution and reproduction in any medium, provided the author and source are cited.

JACS
JOURNAL OF THE AMERICAN CHEMICAL SOCIETY
Article
pubs.acs.org/JACS

Excited-State Relaxation of Hydrated Thymine and Thymidine Measured by Liquid-Jet Photoelectron Spectroscopy: Experiment and Simulation

Franziska Buchner,[†] Akira Nakayama,*[,‡] Shohei Yamazaki,[¶] Hans-Hermann Ritze,[†] and Andrea Lübcke*[,†]

[†]Max-Born-Institut für nichtlineare Optik und Kurzzeitspektroskopie, Max-Born-Straße 2A, 12489 Berlin, Germany

[‡]Catalysis Research Center, Hokkaido University, Sapporo 001-0021, Japan

[¶]Department of Frontier Materials Chemistry, Graduate School of Science and Technology, Hirosaki University, Hirosaki 036-8561, Japan

Supporting Information

ABSTRACT: Time-resolved photoelectron spectroscopy is performed on thymine and thymidine in aqueous solution to study the excited-state relaxation dynamics of these molecules. We find two contributions with sub-ps lifetimes in line with recent excited-state QM/MM molecular dynamics simulations (*J. Chem. Phys.* **2013**, *139*, 214304). The temporal evolution of ionization energies for the excited $\pi\pi^*$ state along the QM/MM molecular dynamics trajectories were calculated and are compatible with experimental results, where the two contributions correspond to the relaxation paths in the $\pi\pi^*$ state involving different conical intersections with the ground state. Theoretical calculations also show that ionization from the $n\pi^*$ state is possible at the given photon energies, but we have not found any experimental indication for signal from the $n\pi^*$ state. In contrast to currently accepted relaxation mechanisms, we suggest that the $n\pi^*$ state is not involved in the relaxation process of thymine in aqueous solution.

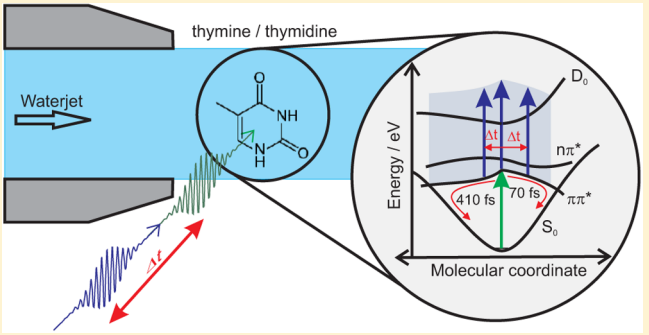

1. INTRODUCTION

DNA bases strongly absorb in the ultraviolet (UV) range and, yet, are astonishingly photostable.[1] The photostability of the DNA bases is discussed to play a key role for the photostability of DNA, itself. The biological relevance of DNA and its photoprotection mechanism triggered extensive research during the last ten years.[1−5] It is nowadays widely accepted that photostability of DNA bases is due to very efficient electronic relaxation via conical intersections with the ground state. Nevertheless, the detailed relaxation paths are still not fully resolved, in particular for the pyrimidine bases (thymine, cytosine, and uracil) there is still a lot of controversy.

Figure 1 shows the low-lying electronic states of isolated and hydrated thymine at the ground-state equilibrium geometry. In the gas phase an intense absorption band corresponding to excitation to the bright $\pi\pi^*$ state centered at 250 nm (4.95 eV)[6] is observed.

In isolated thymine, excited-state decay times of <50 fs, <1 ps, and ∼2.4···6.4 ps are observed.[7] Different interpretations have been suggested. (i) Dynamics on the $S_2(\pi\pi^*)$ surface, where the fs dynamics is due to relaxation to an S_2 minimum, while barrier crossing to the S_2/S_1 conical intersection (CI) is responsible for the ps decay.[8,9] (ii) A barrierless pathway on the $\pi\pi^*$ state from the Franck−Condon (FC) region to an ethylene-like CI with the ground state and trapping of part of the excited-state population in a $\pi\pi^*$ state planar minimum.[10] (iii) A fast transition from $S_2 \rightarrow S_1$ followed by a slower decay $S_1 \rightarrow S_0$.[11] A recent time-resolved Auger spectroscopic study is in support of the last interpretation.[12]

In aqueous solution, due to the interactions with solvent water molecules, the $\pi\pi^*$ state is stabilized, while the $n\pi^*$ state is strongly destabilized with respect to the ground state (see Figure 1)

Around the FC region, the vertical ionization energy in aqueous solution is 8.1 eV[13] associated with a π hole ($D_0(\pi^{-1})$), according to Koopmans' theorem. The vertical ionization energy for ionizing into $D_1(n^{-1})$ is 9.6 eV.[13] In our experiments the total absorbed photon energy is 9.86 eV, indicating that ionization from both excited states is possible in the FC region.

Fluorescence upconversion (FU) experiments in aqueous solution revealed a biexponential sub-ps fluorescence decay, while excited-state absorption decays monoexponentially.[14−16] Transient absorption (TA) studies have also revealed that the vibronic ground state is repopulated with two distinct rates.[17] The faster vibronic ground-state repopulation occurs within a few ps. However, a significant fraction of the vibronic ground state is only populated on a time scale of several tens of ps. The

Received: October 29, 2014
Published: February 11, 2015

© 2015 American Chemical Society

DOI: 10.1021/ja511108u
J. Am. Chem. Soc. 2015, 137, 2931−2938

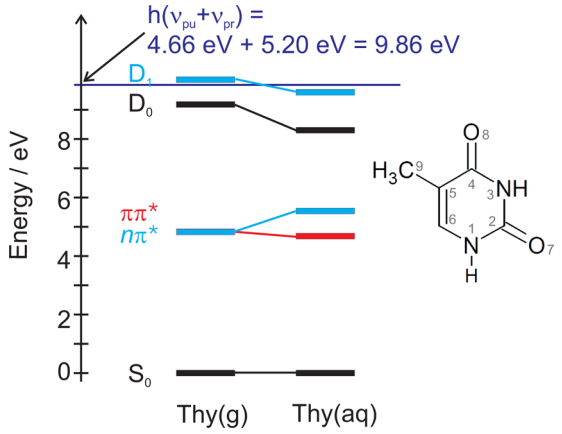

Figure 1. Electronic potential energies of low-lying states of isolated and hydrated thymine around the FC region. Excited-state energies for the gas phase and solvatochromic shift of the nπ^* state are taken from ref 20, and the $\pi\pi^*$ energy of the hydrated molecule is taken from experimental values.[15] Ionization energies for gas phase are taken from ref 22, and ionization energies of hydrated molecules are taken from ref 13. The absorbed photon energy, i.e., the sum of pump photon energy $h\nu_{pu}$ and probe photon energy $h\nu_{pr}$, is given by the horizontal line. The molecular structure and the numbering of the atoms is shown in the right part of the figure.

picture that has emerged from experimental and theoretical findings for the solution phase so far is the excited $\pi\pi^*$ state population very quickly bifurcates: Part of it evolves toward the CI with the ground state, quickly undergoing internal conversion. A significant fraction however is trapped in a long-lived low-lying state, which was suggested to be a close-lying nπ^* state. Based on its lifetime and the fact that this state directly populates the ground state, it was excluded that this dark state is a triplet state.[17] Vibrational cooling of the hot ground state takes about few ps.[17−19]

However, a recent excited-state quantum mechanics/molecular mechanics (QM/MM) molecular dynamics (MD) simulation study suggests that the excited $\pi\pi^*$ state population evolves along two directions: either toward the $(\pi\pi^*(C5{-}C6)/S_0)_{CI}$ involving a twisting of the C5−C6 double bond with a strong puckering of the C6 atom or toward the $(\pi\pi^*(C4{-}O8)/S_0)_{CI}$ which involves an out-of-plane displacement of the C4−O8 carbonyl group[20] (for labeling of the atoms see Figure 1). They also suggested that the nπ^* state is not involved in the excited-state relaxation of thymine in aqueous solution. Very recently, Minezawa investigated the deactivation pathways of thymine in aqueous solution by the combined method of linear-response free energy and collinear spin-flip TD-DFT and found that the free energy of the deactivation pathway through $(\pi\pi^*(C4{-}O8)/S_0)_{CI}$ is significantly stabilized by the solute−solvent interaction[21] supporting the findings of the QM/MM-MD simulation.

In this work, we present the first time-resolved photoelectron studies of thymine (Thy) and its nucleoside thymidine (Thd) in aqueous solution. In Thd, the hydrogen at the N1 position is replaced by a deoxyribose moiety.

2. EXPERIMENTAL SECTION

The experimental setup is described in detail in ref 23. Briefly, the experiment is carried out at a regeneratively amplified Ti:sapphire laser system delivering 40 fs pulses at 800 nm with a 1 kHz repetition rate. Part of the laser power is used to pump an optical parametric amplifier (TOPAS, light conversion). By frequency doubling of the TOPAS output UV pulses in the range of (238···248) nm (5.21···5.00 eV, respectively) are generated. The remaining part is frequency tripled by second harmonic and sum frequency generation in α-BaB_2O_4 (BBO) crystals. UV pulses are attenuated to about 35−40 nJ and focused onto a ∼10 μm thin liquid jet. Both pump and probe beams are chopped allowing for a separate measurement of the one-color photoelectron signals and its subtraction from the two-color signal on a pulse-to-pulse basis. Photoelectrons are collected by a magnetic bottle type time-of-flight (TOF) spectrometer.

The sample is a 0.5 mM aqueous solution of Thy or a 1 mM aqueous solution of Thd, buffered at pH 8 (1 mM tris(hydroxymethyl)-aminomethane (TRIS) and hydrochloric acid (HCl)). In addition, the sample contains 30 mM of sodium chloride (NaCl) to prevent electrokinetic charging of the jet.[24] NaCl does not significantly contribute to the observed one- and two-color signals at the given pulse intensities.[25] DNA bases, nucleosides and TRIS were purchased from Sigma-Aldrich Co., sodium chloride from Merck. All substances were used without further purification. The sample solution was prepared using demineralized water (residual resistivity: 0.25 μS/cm).

3. COMPUTATIONAL SECTION

The QM/MM-MD simulations are performed both in the ground and excited states of a thymine molecule solvated in water. The QM region is composed of the thymine molecule and treated by ab initio calculations, while the MM region consists of surrounding solvent water molecules that are represented by the SPC/Fw model.[26] The electrostatic interaction of electrons in the QM region with the MM effective point charges are taken into account through one-electron integrals. The periodic supercell with a length of 16 Å is employed and the thymine molecule is solvated by 122 water molecules, where the number of water molecules is determined to reproduce the density of water at ambient conditions. The long-range electrostatic interactions between the MM molecules are treated by the Ewald sum and the cutoff distance of 8 Å (half the length of the supercell) is employed for electrostatic interactions between the QM (thymine) and MM molecules. All quantum chemical calculations are performed by the MOLPRO2010.1 package,[27] and it is interfaced with the in-house MD program for the QM/MM-MD simulations.

The QM/MM-MD simulations in the electronic ground state are performed to estimate the vertical excitation and ionization energies in aqueous solution. The Møller−Plesset second-order perturbation (MP2) method with the DZP quality of basis set are employed in the MD simulations. The Newtonian equation of motion for nuclei is integrated by the velocity Verlet algorithm with a time step of 0.5 fs and the temperature is controlled at 300 K by the Nosé−Hoover thermostat. The configurations are picked up at every 250 fs from the MD trajectories, and the complete active space second-order perturbation theory (CASPT2) method is employed to calculate the vertical excitation and ionization energies at these configurations. Then, the averages over 100 configurations are taken to estimate the excitation and ionization energies in aqueous solution, which are used to calculate the constant shift for excited-state ionization energy (see below).

The excited-state QM/MM-MD simulations are performed at the CASPT2 level of theory. The initial coordinates and velocities are taken from the above-mentioned ground-state QM/MM-MD run by picking up coordinates and velocities at every 500 fs. The excited-state MD simulations are performed without the thermostats, and they are initiated from the lowest $\pi\pi^*$ state. When the energy difference between the ground and $\pi\pi^*$ states becomes less than 0.2 eV, we assume that the molecule reaches the CI region.

DOI: 10.1021/ja511108u
J. Am. Chem. Soc. 2015, 137, 2931−2938

Here we describe the details of the CASPT2 calculations. The DZP quality of basis sets are also employed, and a level shift with a value of 0.2 a.u. (~5.4 eV) is applied. The notation of CASPT2(m,n) is occasionally used, in which case the active space for a reference state-averaged complete active space self-consistent field (SA-CASSCF) wave function is composed of m electrons and n orbitals (SA-CASSCF(m,n)). The excited-state QM/MM-MD simulations in the $\pi\pi^*$ state are carried out by CASPT2(4,4), where the active space is comprised of only π orbitals and the lowest two states are averaged with equal weights in the SA-CASSCF calculations. In the previous paper, it was confirmed that the CASPT2(4,4) method provides a reliable description of the $\pi\pi^*$ state.[20] Along the excited-state MD trajectories, the CASPT2(12,9) calculations are performed at fixed intervals to obtain the energies of the ground, lowest $\pi\pi^*$, and $n\pi^*$ states. Here, the active space is comprised of eight π orbitals (five π orbitals are doubly occupied and three are unoccupied in the closed-shell configuration) and one lone-pair orbital that belongs to the O8 atom. The ground, $\pi\pi^*$, and $n\pi^*$ states (a total of three states) are averaged with equal weights in the SA-CASSCF(12,9) calculations. Obviously, our simulations focus on the deactivation process occurring only in the $\pi\pi^*$ state, and the transition from the $\pi\pi^*$ to $n\pi^*$ state is not taken into account. However, the relative energies of the $n\pi^*$ state are obtained along the trajectories, and the role of the $n\pi^*$ state is discussed in section 5.

The cationic ground and first excited states (D_0 and D_1), which correspond to either π-hole or n-hole states, are also calculated by the CASPT2 method along the QM/MM-MD trajectories. The active space is the same as that used in the calculations of the neutral molecule, except that the number of electrons in the active space is 11 in this case, and therefore it can be denoted by CASPT2(11,9). Here, two states, D_0 and D_1, are averaged with equal weights in the reference SA-CASSCF(11,9) calculations.

At this point we should comment on the relative stability of the lowest $\pi\pi^*$ and $n\pi^*$ states around the FC region. In the gas phase, theoretical calculations predicted that the lowest $\pi\pi^*$ and $n\pi^*$ states lie close to each other and the order of these two state changes depending on the computational levels. The literature values before 2008 are compiled in ref 28, and the more recent values are found in our previous paper.[20] In aqueous solution, the $\pi\pi^*$ state is stabilized, while the $n\pi^*$ state is strongly destabilized due to the hydrogen bond with solvent water molecules. This destabilization of the $n\pi^*$ state is rationalized by recognizing that the electronic transition involves the transfer of an electron in the lone-pair orbital of the O8 atom, which acts as a hydrogen-bond acceptor, toward the diffusive π^* orbital, leading to a decrease in the solute−solvent interaction. Because of this, for both thymine and uracil, it is generally accepted that the $n\pi^*$ state is less stable than the $\pi\pi^*$ state around the FC region in aqueous solution (see a recent review by Improta and Barone[5]). Specifically, for thymine, the time-dependent density functional theory (TD-DFT) calculations employing explicit four water molecules and polarizable continuum models predicted that the vertical excitation energies are 4.97 (−0.09) and 5.27 (+0.41) eV for the lowest $\pi\pi^*$ and $n\pi^*$ states, respectively (the numbers in parentheses indicate the shifts from the gas-phase values).[15] Also, Etinski and Marian employed six water molecules in conjunction with the conductor-like screening model (COSMO) and the excitation energies obtained by the coupled cluster with approximate treatment of doubles (CC2) method were 5.08 (−0.18) and 5.48 (+0.51) eV for the $\pi\pi^*$ and $n\pi^*$ excitations, respectively.[29] Our calculated values by the QM(CASPT2)/MM-MD approach are 4.47 (−0.30) and 5.41 (+0.54) eV for the $\pi\pi^*$ and $n\pi^*$ excitations, respectively, and it is seen that the $\pi\pi^*$ excitation energy is closer to the experimental value of 4.68 eV[15] than other theoretical works. Also, the shift from the gas-phase value for the $\pi\pi^*$ excitation is in quite good agreement with the experiment (−0.27 eV).[6,15]

As often pointed out before, the accuracy of the ionization energy and the excitation energy is not similar. Therefore, the excited-state ionization potential energy is corrected using the experimental value, as has been done before.[8,30] Here, the constant shift Δ is introduced, which is adjusted to ensure that the calculated excited-state ionization energy matches with the experimental value, and is given by

$$\Delta = \langle E^{\mathrm{CASPT2}}_{\mathrm{D}_0(\pi^{-1})} - E^{\mathrm{CASPT2}}_{\mathrm{S}_0}\rangle_{\mathrm{aq}} - \langle E^{\mathrm{CASPT2}}_{\mathrm{S}_1(\pi\pi^*)} - E^{\mathrm{CASPT2}}_{\mathrm{S}_0}\rangle_{\mathrm{aq}} - (IE^{\mathrm{vertical,expt,aq}}_{\mathrm{S}_0\rightarrow\mathrm{D}_0(\pi^{-1})} - \Delta E^{\mathrm{vertical,expt,aq}}_{\mathrm{S}_0\rightarrow\mathrm{S}_1(\pi\pi^*)}) \quad (1)$$

where S_0 is the neutral ground state and D_0 is the cationic ground state. When the thymine molecule is equilibrated in aqueous solution, D_0 is associated with the π-hole cation. The averages of the $S_1(\pi\pi^*)$ vertical excitation and ionization energies in aqueous solution are calculated to be $\langle E^{\mathrm{CASPT2}}_{\mathrm{S}_1(\pi\pi^*)} - E^{\mathrm{CASPT2}}_{\mathrm{S}_0}\rangle_{\mathrm{aq}} = 4.47$ eV and $\langle E^{\mathrm{CASPT2}}_{\mathrm{D}_0(\pi^{-1})} - E^{\mathrm{CASPT2}}_{\mathrm{S}_0}\rangle_{\mathrm{aq}} = 8.74$ eV, respectively, where the computational details are given above. By using the experimental values of $IE^{\mathrm{vertical,expt,aq}}_{\mathrm{S}_0\rightarrow\mathrm{D}_0(\pi^{-1})} = 8.1$ eV[13] and $\Delta E^{\mathrm{vertical,expt,aq}}_{\mathrm{S}_0\rightarrow\mathrm{S}_1(\pi\pi^*)} = 4.68$ eV,[15] we find $\Delta = 0.85$ eV for the correction of the excited-state ionization potential energy in aqueous solution.

In order to examine the possibility of detecting the signal if the molecule is trapped in the $n\pi^*$ state, we have also run the QM/MM-MD simulations in the $n\pi^*$ state by employing the SA-CASSCF(12,9) method. In the CASSCF method, the potential energy of the $\pi\pi^*$ state is usually highly overestimated, and therefore even in aqueous solution, the S_1 state is characterized by the $n\pi^*$ state. After running several picoseconds in the $n\pi^*$ state, the molecule is equilibrated in the $n\pi^*$ state. Then we further run additional 5 ps, and we use CASPT2 calculations along these trajectories and evaluate the ionization energies from the $n\pi^*$ state.

We note that the electron correlation effects are different between the $\pi\pi^*$ and $n\pi^*$ states, and therefore when evaluating the excited-state ionization energy, it is advisible to use different shifts depending on which excited state the ionization occurs. In obtaining a shift for the ionization from the $n\pi^*$ state, however, no experimental values of the $S_2(n\pi^*)$ vertical excitation energy $\Delta E^{\mathrm{vertical,expt,aq}}_{\mathrm{S}_0\rightarrow\mathrm{S}_2(n\pi^*)}$ are available. The experimental value of the ionization energy to the $D_1(n^{-1})$ state is given as $IE^{\mathrm{vertical,expt,aq}}_{\mathrm{S}_0\rightarrow\mathrm{D}_1(n^{-1})} = 9.6$ eV,[13] and our theoretical values of the ionization energy to the $D_1(n^{-1})$ state and the $S_2(n\pi^*)$ vertical excitation energy are $\langle E^{\mathrm{CASPT2}}_{\mathrm{D}_1(n^{-1})} - E^{\mathrm{CASPT2}}_{\mathrm{S}_0}\rangle_{\mathrm{aq}} = 10.55$ eV and $\langle E^{\mathrm{CASPT2}}_{\mathrm{S}_2(n\pi^*)} - E^{\mathrm{CASPT2}}_{\mathrm{S}_0}\rangle_{\mathrm{aq}} = 5.41$ eV, respectively. Therefore, the shift is given as $\Delta = \Delta E^{\mathrm{vertical,expt,aq}}_{\mathrm{S}_0\rightarrow\mathrm{S}_2(n\pi^*)} - 4.46$ eV. It is known that the CASPT2 method tends to overestimate the electron correlation of the $\pi\pi^*$ state for DNA bases (e.g., see Table 1 in ref 31) and this fact is reflected in the lower $\pi\pi^*$ excitation energy than the experiment: 4.95 eV (experiment) and 4.77 eV (CASPT2) in the gas phase. Since the electron correlation in the $\pi\pi^*$ state is generally stronger than that in the $n\pi^*$ state, we speculate that the calculated $n\pi^*$ excitation energy is closer to the experimental value (if available) than the $\pi\pi^*$ state. Therefore, if we assume that $\Delta E^{\mathrm{vertical,expt,aq}}_{\mathrm{S}_0\rightarrow\mathrm{S}_2(n\pi^*)}$ is the same as the calculated value, the shift is estimated as $\Delta = 0.95$

DOI: 10.1021/ja511108u
J. Am. Chem. Soc. 2015, 137, 2931−2938

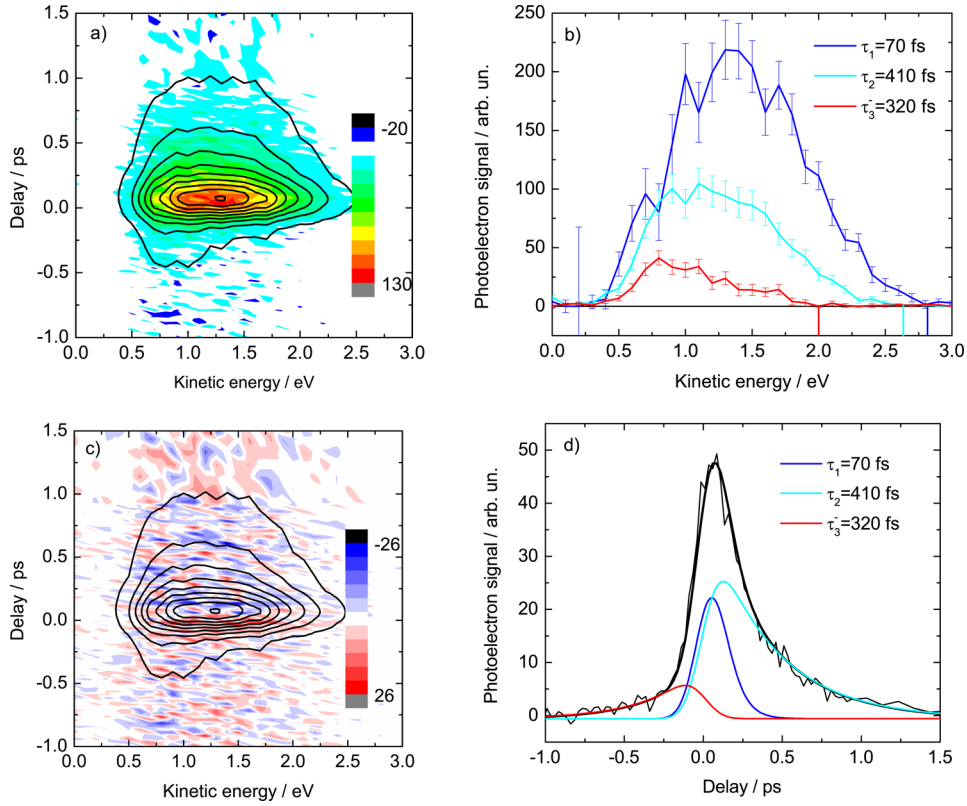

Figure 2. Time-resolved photoelectron spectrum of thymine, globally analyzed by three spectral contributions. (a) Comparison between data (color) and global fit (contour lines), (b) decay associated spectra, (c) residuals (color) and global fit (contour lines), and (d) population dynamics of individual contributions. The color scale of the residuals covers a range of ±20% of the maximum photoelectron signal. Vertical lines in panel b mark the maximum kinetic energies for the individual contributions.

eV, which is slightly larger than the shift for the $\pi\pi^*$ state of Δ = 0.85 eV. We use the shift of Δ = 0.85 eV throughout this work, but given this small difference of the shifts (~0.1 eV), the discussion of the ionization from the $n\pi^*$ state given below will not be affected.

4. RESULTS

Figure 2 shows the time-dependent photoelectron spectra and the global fit results for Thy. Results for Thd are shown in Figure S4 in the Supporting Information.[32] Photoelectrons are generated, if the probe pulse photon energy is larger than the time-dependent ionization energy of the excited molecule. Therefore, the signal decay can in principle reflect the excited state population decay, an increase of the energy gap between excited neutral state and final ionic state exceeding the probe photon energy, and time-dependent ionization cross sections. This has to be kept in mind when discussing the observed lifetimes.

We observe photoelectron signal from the excited molecules for kinetic energies up to about 2.5 eV and for a delay range $\Delta\tau$ of $-0.5\ \text{ps} \leq \Delta\tau \leq 1\ \text{ps}$. Signal at positive (negative) delays originates from photoreaction triggered by the pulse at 266 nm (238 nm) and probed by 238 nm (266 nm). A global analysis of the data was performed by fitting with the following function:

$$N(E_{\text{kin}}, t) = \sum_i A_i(E_{\text{kin}})[P_i(t) \otimes G(t)] \tag{2}$$

$A_i(E_{\text{kin}})$ is the decay associated spectrum and $P_i(t)$ is the excited-state population of the ith contribution, while $G(t)$ is the Gaussian cross-correlation function.

In a first attempt, the data were analyzed in terms of only a single exponential excited-state population decay for each delay direction. These results are shown in Figures S3 and S4 in the Supporting Information. Although this model fits the data quite reasonably, there are systematic residuals. Therefore, the experimental results were analyzed based on a model that assumes two parallel relaxation paths:

$$S_0 \xrightarrow{\hbar\omega} \begin{cases} S_m \xrightarrow{k_1} S_0 \\ S_n \xrightarrow{k_2} S_0 \end{cases} \tag{3}$$

S_m and S_n may be different excited states or refer to different trajectories on the same excited-state potential energy surface. Please note that by parallel relaxation path we mean the temporal evolution of wave packets generated at two different points in phase space. For negative delays we used only one relaxation path (see below for the discussion). For comparison, the Supporting Information shows also results, in which two components in each delay direction are considered. Following the analysis of Ullrich et al.,[7] we assume in our global analysis that the spectra of the two components do not change in time. The cross-correlation width (220 fs fwhm) and the temporal origin t_0 were independently determined from nonresonant two-color photoelectron signal of gaseous nitric oxide (NO) and buffer solution. At long delay times we observe a very small negative pump probe signal (the same at positive and negative delays), which we attribute to dead time effects of the multi channel plate in single electron counting mode. This is included in the fit by a temporally constant negative contribution. The fit result together with the data are

DOI: 10.1021/ja511108u
J. Am. Chem. Soc. 2015, 137, 2931−2938

Table 1. Summary of Fit Parameters and Comparison with Fluorescence Upconversion Results[14,15a]

		τ_1/fs	τ_2/fs	τ_t/ps	τ_3^-/fs	α	β
this work	Thy	70 ± 10	410 ± 40		320 ± 40	0.69	0.08
	Thd	120 ± 10	390 ± 10		290 ± 20	0.54	0.09
FU	Thy[15]	195 ± 17	633 ± 18			0.56 ± 0.02	
	Thd[33]	150 ± 20	720 ± 30			0.70 ± 0,02	
TA	Thy[16,17]		540 ± 40[b]	30 ± 13		0.77	

[a] $\tau_{1\text{-}3}$ are derived lifetimes, where the superscript "−" refers to the value obtained for negative delay direction. $A_i = \int_0^\infty A_i(E_{kin})\, dE_{kin}$ is the energy integrated signal associated with decay i at delay = 0. $\alpha = (A_1^+)/(A_1^+ + A_2^+)$ is the fraction of the signal of the faster decaying component A_1^+ in the total signal $A_1^+ + A_2^+$ in positive delay direction. $\beta = (A^-)/(A_1^+ + A_2^+)$ is the ratio between signal in negative delay direction A^- to signal in positive delay direction $A_1^+ + A_2^+$. Uncertainties given correspond to one standard deviation as obtained from the fit. [b] Thd.

shown in Figure 2a, while Figure 2c shows the residuals of the global analysis. Fit parameters are summarized in Table 1.

At positive delays, the residuals mainly reflect statistical deviations of the data and the model fits the experiment very well. However, at negative delays close to the temporal overlap, residuals are systematically positive (in particular for Thd, see Figure S4 in the Supporting Information[32]), indicating that the model underestimates the excited-state signal. It becomes evident from Figures 2d and S4k in the Supporting Information[32] that the deviations seem to arise from a very tiny temporal shift of the excited-state population decay which may simply reflect the limitations of an exponential decay model. Instead, the prepared wave packet needs some time to evolve and to reach the CI; that is, it is reasonable to expect a small delay in excited-state depopulation.

The decay associated spectra are shown in Figure 2b and the population dynamics of the individual contributions in Figure 2d. In positive delay direction we observe contributions with lifetimes of 70 fs (120 fs) and 410 fs (390 fs) for Thy (Thd). These lifetimes are shorter than those obtained in FU or TA experiments (cf. Table 1). As mentioned above, possible reasons are the energy gap betweeen the excited and ionic state exceeding the probe photon energy or time-dependent ionization cross sections. However, also the observed lifetimes in TA or FU may be influenced from time-dependent cross sections, overlapping features (e.g., hot ground state absorption), and a direct comparison is difficult. The lifetimes we have retrieved for Thy are slightly shorter than for Thd and thus seem to follow the opposite trend than observed in TA and FU. However, we stress that in all cases the given errors are from the fit, only. Due to the rather long cross-correlation or instrumental response functions, the real errors should be expected much larger in either case.

The average kinetic energies

$$\mathrm{AKE} = \frac{\int_0^\infty I(E_{kin}) E_{kin} dE_{kin}}{\int_0^\infty I(E_{kin}) dE_{kin}} \quad (4)$$

for Thy (Thd) are 1.42 eV (1.43 eV) for the faster decaying component and 1.26 eV (1.19 eV) for the second component. For negative delays the excited-state lifetime is 320 fs (290 fs) and the AKE is 1.08 eV (1.00 eV). Apparently, the kinetic energy difference between the contributions at positive delays and the one at negative delays does not correspond to the probe photon energy difference (5.2 − 4.66 eV = 0.54 eV). We have previously observed, that the photoelectron signal at very low kinetic energies in liquid jet experiments is in general strongly reduced, possibly as an effect of a cloud of charged water clusters surrounding the liquid jet.[24,25] This would lead to an overestimation of AKE values, in particular for the lower probe photon energy case of negative delay directions. Similar behavior was observed in case of adenine and adenosine, where additional photoelectron band broadening effects were explained by wave packet dynamics within the pulse duration. In case of adenine/adenosine we have shown, that the difference of maximum kinetic energies is in good agreement with the probe photon energy difference.[25] For Thy (Thd), the maximum kinetic energies of the individual contributions are 2.8 eV (2.9 eV) and 2.6 eV (2.6 eV) at positive delays and 2.0 eV (2.0 eV) at negative delays (cf. Figures 2b and S4h in the Supporting Information[32]).

The difference between the maximum kinetic energy for the slower decaying component at positive delays and the component in negative direction fits very well with the difference in probe photon energy which indicates that both contributions originate from the same relaxation path. This, in turn, would indicate the absence of the faster decay in the negative direction. However, the low signal at negative delays makes the deconvolution very difficult, and we cannot exclude that both components contribute to the signal here.

We have also performed a global analysis assuming four contributions, i.e., two in each direction. This analysis gives similarly good results as with three components only (see the Supporting Information[32]). For Thy we find very similar decay rates at negative and positive delays, although the additional, quickly decaying component has only a very small share in the entire signal. In Thd, the contribution is even smaller, and its retrieved lifetime (3 fs) is unrealistically small. In conlusion, considering three contributions for the global analysis of our data is reasonable, in particular if the main focus is on the dynamics in positive delays. The overall similarity between the spectra and observed decay times obtained for Thy and Thd leads to the conclusion that the excited-state relaxation occurs along the same coordinates in both molecules.

If the molecules are excited at 238 nm (negative delays), the observed excited-state signal decays with a lifetime of 300 fs, i.e., 100 fs faster than in case of 266 nm excitation. This may reflect both accelerated excited-state dynamics due to higher excess energy or a smaller FC window for ionization due to lower probe photon energy, i.e., the accessible phase space for observation of the excited state is smaller at negative than at positive delays.

5. ASSIGNMENT OF THE RELAXATION PATHS

Our data show that the excited-state dynamics of Thy and Thd after optical excitation at 4.66 eV involve two components and occur on sub-ps time scales. No experimental evidence for a trapped excited-state population persisting as long as 30 ps is observed. Given the electron effective attenuation length in liquid water of 2−5 nm at low kinetic energies,[34−37] an assignment of the two observed contributions to dynamics occurring in molecules in the bulk or at the surface may be

DOI: 10.1021/ja511108u
J. Am. Chem. Soc. 2015, 137, 2931−2938

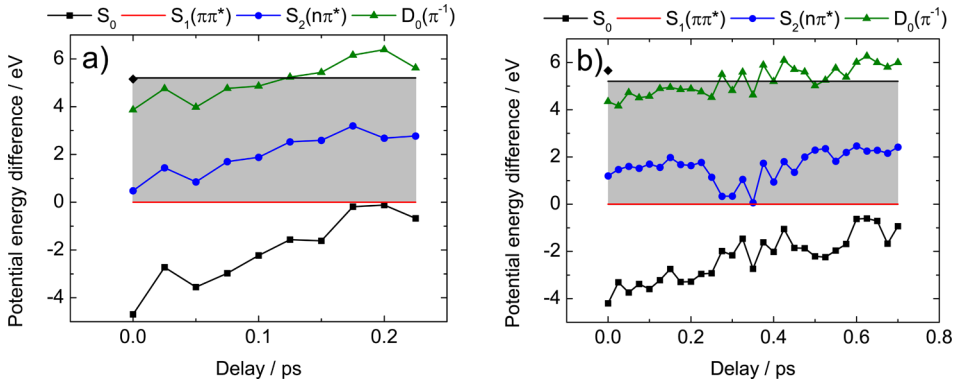

Figure 3. Potential energy differences between the $\pi\pi^*$ state and the neutral ground state, the $n\pi^*$ state and the ionic ground state along representative trajectories taken from ref 20 that reach $(\pi\pi^*(C5{-}C6)/S_0)_{CI}$ (left) and $(\pi\pi^*(C4{-}O8)/S_0)_{CI}$ (right) regions. Gray-shaded areas (between red and black solid lines) show ionization windows of $\pi\pi^*$ state for instantaneous and complete redistribution of excess energy ($E(\pi\pi^*) + \hbar\omega_{pr}$) in case of 5.2 eV probe pulses. Diamonds mark the total absorbed energy at temporal overlap ($\hbar\omega_{pu} + \hbar\omega_{pr} + E(S_0; t = 0)$).

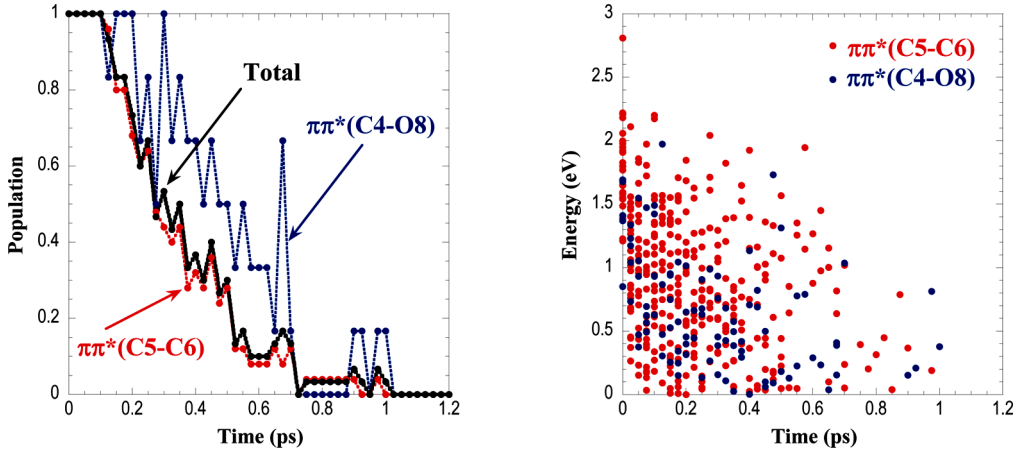

Figure 4. (left) Average population of trajectories in the $\pi\pi^*$ state that can be ionized for the given pump−probe time delay and photon energy ($\hbar\omega_{pr}$ = 5.2 eV) (black line). The trajectories are divided into two groups: trajectories that reach the $(\pi\pi^*(C5{-}C6)/S_0)_{CI}$ and $(\pi\pi^*(C4{-}O8)/S_0)_{CI}$ regions, and the average populations of each group are shown in blue and red dotted lines. (right) Kinetic energies of photoelectrons along the trajectories. The trajectories are again divided into two groups and shown in blue and red circles. The averages of kinetic energy at $t = 0$ over all trajectories are calculated to be 1.72 eV. The averages over trajectories that reach the $(\pi\pi^*(C5{-}C6)/S_0)_{CI}$ and $(\pi\pi^*(C4{-}O8)/S_0)_{CI}$ regions are 1.80 and 1.40 eV, respectively.

conceivable. However, we discard this assignment. A detailed discussion is found in the Supporting Information.[32]

Can the two observed pathways be assigned to the different pathways observed in recent QM/MM-MD simulations?[20] What is the role of the $n\pi^*$ state for the excited-state dynamics?

We have performed QM/MM-MD simulations as described in ref 20 but extended the calculations to 30 trajectories. We found 6 trajectories reaching $(\pi\pi^*(C4{-}O8)/S_0)_{CI}$ and 24 reaching ethylene-like $(\pi\pi^*(C5{-}C6)/S_0)_{CI}$ regions. For the ethylene-like relaxation paths, the $n\pi^*$ state is always above the $\pi\pi^*$ state (see the Supporting Information, Figure S7(left)[32]). For the trajectories that reach $(\pi\pi^*(C4{-}O8)\ /S_0)_{CI}$ regions, the $n\pi^*$ state sometimes gets close to the $\pi\pi^*$ state (see the Supporting Information, Figure S7(right)[32]). In our simulation, we cannot treat the hopping from the $\pi\pi^*$ to the $n\pi^*$ state. But if the transition to the $n\pi^*$ state takes place, then the molecule will relax to the equilibrium structure in the $n\pi^*$ state. We will show below that the photon energy of the probe pulse is large enough to ionize the equilibrated molecule in the $n\pi^*$ state. We notice that in Figure S7(right) the S_0, $\pi\pi^*$, and $n\pi^*$ states come close to each other at some points, suggesting the existence of the three-state conical intersections around that region. The involvement of the three-state conical intersections in the relaxation dynamics of pyrimidine bases has been previously proposed.[38−40]

In Figure 3 we show the temporal evolution of the potential energy difference between the $\pi\pi^*$ state and the ground state S_0, the $n\pi^*$ excited state as well as the ionic ground state $D_0(\pi^{-1})$ along representative trajectories toward either conical intersection region.

In addition, we show also the energetic range that can be overcome by absorption of a probe pulse photon for the case that the excess energy is completely and instantaneously distributed over different modes. We find that the molecule can be ionized along a significant fraction of the relaxation paths. Given the typically very broad photoelectron bands, we do expect to detect photoelectrons during the entire residence of the molecule in the $\pi\pi^*$ state.

It is interesting to compare the decay associated spectra with the electron kinetic energies calculated for the relaxation along the two pathways. In Figure 4 (right panel) we show photoelectron kinetic energies along the individual trajectories.

For relaxation toward $(\pi\pi^*(C5{-}C6)/S_0)_{CI}$, we find an average kinetic energy of 1.8 eV at temporal overlap. The ionization energy very quickly increases as nuclear dynamics sets in. Already after 25 fs, the average kinetic energy is only about 1

DOI: 10.1021/ja511108u
J. Am. Chem. Soc. 2015, 137, 2931−2938

eV. For comparison with experimental data we need to consider our limited temporal resolution. Averaging over the first 100 fs from simulations we find an average photoelectron kinetic energy of 1.14 eV. For the relaxation toward $(\pi\pi^*(C4-O8)/S_0)_{CI}$, the average kinetic energy at $t = 0$ is 1.4 eV, averaging over the first 100 fs, it amounts to 1.05 eV. The temporally averaged values are slightly smaller than derived from our experiments. However, as discussed before, we expect to measure larger average kinetic energies due to reduced photoelectron signal at low kinetic energies. Considering this aspect, the difference between the average kinetic energies found from the simulation and experiment are in good agreement. Also, the amplitude ratios of the two relaxation paths found in experiment and simulation are in good agreement: In the simulation, 20% of the trajectories proceed toward $(\pi\pi^*(C4-O8)/S_0)_{CI}$, while 80% reach $(\pi\pi^*(C5-C6)/S_0)_{CI}$. In the experiment we find an amplitude ratio of about 30:70 for the two components. Figure 4 (left panel) shows the excited-state population which can be ionized by the probe photon energy as retrieved from the simulations. We find that the ethylene-like path leads to faster internal conversion than the path toward $(\pi\pi^*(C4-O8)/S_0)_{CI}$; nevertheless, both relaxation paths take place on a sub-ps time scale. Based on the qualitative agreement of the photoelectron spectrum, the relative amplitudes and the excited-state lifetime, between QM/MM-MD simulations and experiment we assign the short-lived component to a wave packet following the ethylene-like relaxation path and the longer-lived component to a wave packet which proceeds toward $(\pi\pi^*(C4-O8)/S_0)_{CI}$.

Is the $n\pi^*$ state involved in the relaxation dynamics?

As mentioned previously, our simulation can not treat the hopping from the $\pi\pi^*$ to the $n\pi^*$ state. If such a transition occurs, the molecule will relax to the $n\pi^*$ minimum. We will show here, that the photon energy of the probe pulse (5.2 eV) is high enough to ionize the molecule equilibrated in the $n\pi^*$ state. We have run QM/MM-MD simulations in the $n\pi^*$ state in aqueous solution (see the Computational section) and found that the ionization energies from the $n\pi^*$ state to $D(n^{-1})$ or $D(\pi^{-1})$ (n-hole is not always the cationic ground state along trajectories, n-hole and π-hole states switch often) along the trajectories are close to and on average slightly below the photon energy of the probe pulse (see Figure 5).

Ionizing the molecule in the $n\pi^*$ state removes the electron from the π^* orbital, i.e., due to the charater of the electronic configuration in the single-electron transition, we expect predominantly ionization into the $D(n^{-1})$ ionic state, leaving an n-hole in the molecule.[41] Therefore, contributions from ionization into $D(\pi^{-1})$ are expected to be small. Considering the typically very broad photoelectron bands of hydrated molecules, we would clearly expect to detect photoelectrons from molecules trapped in the $n\pi^*$ state.

This would have been visible in particular at longer delays, when the $\pi\pi^*$ population has decayed. From the absence of any long-lived signal, we conclude that the $n\pi^*$ state does not play an important role in the relaxation process. The biexponential repopulation of the vibronic ground state observed in transient absorption[17] might instead reflect ground state dynamics along different relaxation paths. We want to note that also in the case of cytosine and its nucleoside we do not observe any contribution from the $n\pi^*$ state, although the ionization energies are significantly lower for the $n\pi^*$ state; that is, the ionization window is significantly larger, and also in spite of the fact that at least for Cyt nucleotide the dark state yield was reported to be 41%.[17]

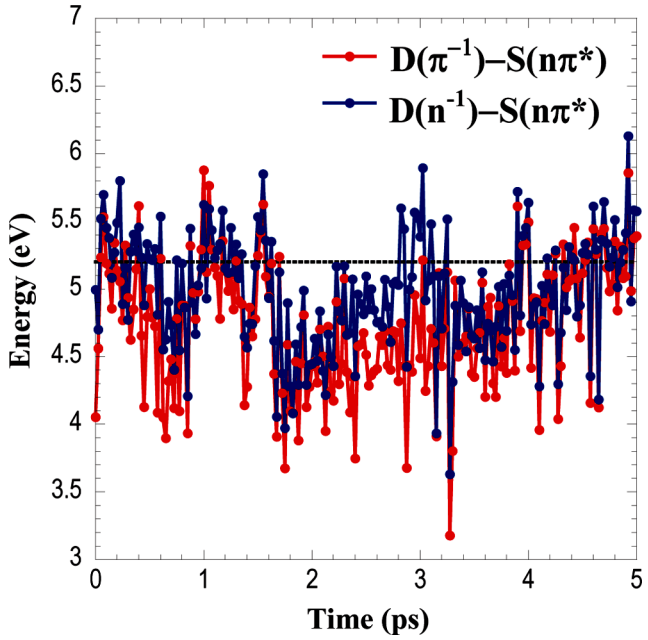

Figure 5. Potential energy difference between the $D(\pi^{-1})$ and $n\pi^*$ states (red line), and the $D(n^{-1})$ and $n\pi^*$ states (blue line) along the QM/MM-MD trajectories that are equilibrated in the $n\pi^*$ state using the SA-CASSCF(12,9) calculations. The energies are recalculated by CASPT2-(12,9) and CASPT2(11,9) for the neutral and cationic molecules, respectively. The energies of the cationic states are shifted using the correction described in the text, and the experimentally applied photon energy (5.2 eV) is shown by the dotted line.

6. CONCLUSIONS

We have followed the $\pi\pi^*$ population excited by short UV pulses in thymine and thymidine. In agreement with recent excited-state QM/MM-MD simulations we find two different relaxation paths toward conical intersections with the ground state.[20] These relaxation paths are assigned to an ethylene-like relaxation toward the $(\pi\pi^*(C5-C6)/S_0)_{CI}$ and toward $(\pi\pi^*(C4-O8)/S_0)_{CI}$ regions. When molecules are excited by 266 nm light (4.66 eV) excited-state lifetimes of thymine (thymidine) are 70 fs (120 fs) and 410 fs (390 fs), respectively. These lifetimes are somewhat shorter than observed in fluorescence upconversion or in our QM/MM-MD simulations (see Figure 4, left panel).

No contribution from the $n\pi^*$ excited state has been observed, although we have shown that the probe photon energy is sufficiently high to ionize the equilibrated molecule in the $n\pi^*$ state. From the absence of any long-lived signal we conclude that the $n\pi^*$ state is very likely not involved in the excited-state relaxation of Thy and Thd. We may speculate that in this case, the biexponential repopulation of the vibronic ground state observed in transient absorption[17] reflects ground-state dynamics along different relaxation paths.

Finally, we want to note that similar data are available for cytosine which will be discussed in a separate paper. Also for cytosine, the signal from the $n\pi^*$ state is absent, although cytosine has a significantly larger ionization window due to lower ionization energies.

Our work shows the potential of liquid jet time-resolved photoelectron spectroscopy to study the excited-state dynamics of solvated molecules in dilute solutions. It provides important new information complementary to transient absorption or fluorescence upconversion and will thus contribute significantly

DOI: 10.1021/ja511108u
J. Am. Chem. Soc. 2015, 137, 2931−2938

to a better understanding of excited-state dynamics of solvated molecules and, in particular, of hydrated DNA bases.

■ ASSOCIATED CONTENT

Supporting Information

Details on the detection efficiency at low kinetic energy, the role of inelastic processes, global analysis, time-resolved photoelectron spectra, global analysis results for thymine and thymidine, an extended time scan for thymine, and a discussion of alternative signal assignment. This material is available free of charge via the Internet at http://pubs.acs.org.

■ AUTHOR INFORMATION

Corresponding Authors

*E-mail: nakayama@cat.hokudai.ac.jp.
*E-mail: luebcke@mbi-berlin.de.

Notes

The authors declare no competing financial interest.

■ ACKNOWLEDGMENTS

The authors thank F. Noack for his support by providing the laser system in the femtosecond application laboratory of the Max-Born-Institut Berlin. This work was financially supported by Deutsche Forschungsgemeinschaft, Project LU 1638/1-1, and by KAKENHI (Grant-in-Aid for Scientific Research). Part of the calculations was performed on supercomputers at Research Center for Computational Science, Okazaki, Japan.

■ REFERENCES

(1) Crespo-Hernández, C. E.; Cohen, B.; Hare, P. M.; Kohler, B. *Chem. Rev.* **2004**, *104*, 1977.
(2) de Vries, M. S.; Hobza, P. *Annu. Rev. Phys. Chem.* **2007**, *58*, 585.
(3) Middleton, C. T.; de La Harpe, K.; Su, C.; Law, Y. K.; Crespo-Hernández, C. E.; Kohler, B. *Annu. Rev. Phys. Chem.* **2009**, *60*, 217.
(4) Kleinermanns, K.; Nachtigallová, D.; de Vries, M. S. *Int. Rev. Phys. Chem.* **2013**, *32*, 308.
(5) Improta, R.; Barone, V. *Top. Curr. Chem.* **2014**, *355*, 329.
(6) Abouaf, R.; Pommier, J.; Dunet, H. *Chem. Phys. Lett.* **2003**, *381*, 486.
(7) Ullrich, S.; Schultz, T.; Zgierski, M. Z.; Stolow, A. *Phys. Chem. Chem. Phys.* **2004**, *6*, 2796.
(8) Hudock, H. R.; Levine, B. G.; Thompson, A. L.; Satzger, H.; Townsend, D.; Gador, N.; Ullrich, S.; Stolow, A.; Martínez, T. J. *J. Phys. Chem. A* **2007**, *111*, 8500.
(9) Szymczak, J. J.; Barbatti, M.; Hoo, J. T. S.; Adkins, J. A.; Windus, T. L.; Nachtigallová, D.; Lischka, H. *J. Phys. Chem. A* **2009**, *113*, 12686.
(10) Merchán, M.; González-Luque, R.; Climent, T.; Serrano-Andrés, L.; Rodríguez, E.; Reguero, M.; Peláez, D. *J. Phys. Chem. B* **2006**, *110*, 26471.
(11) Lan, Z.; Fabiano, E.; Thiel, W. *J. Phys. Chem. B* **2009**, *113*, 3548.
(12) McFarland, B. K.; Farrell, J. P.; Miyabe, S.; Tarantelli, F.; Aguilar, A.; Berrah, N.; Bostedt, C.; Bozek, J. D.; Bucksbaum, P. H.; Castagna, J. C.; Coffee, R. N.; Cryan, J. P.; Fang, L.; Feifel, R.; Gaffney, K. J.; Glownia, J. M.; Martinez, T. J.; Mucke, M.; Murphy, B.; Natan, A.; Osipov, T.; Petrovíc, V. S.; Schorb, S.; Schultz, T.; Spector, L. S.; Swiggers, M.; Tenney, I.; Wang, S.; White, J. L.; White, W.; Gühr, M. *Nat. Comm.* **2014**, *5*, 4235.
(13) Seidel, R. Electronic-Structure Interactions in Aqueous Solutions: A Liquid-Jet Photoelectron-Spectroscopy Study. Ph.D. Thesis; Technische Universitaet Berlin: Berlin, 2011.
(14) Gustavsson, T.; Sharonov, A.; Markovitsi, D. *Chem. Phys. Lett.* **2002**, *351*, 195.
(15) Gustavsson, T.; Bányász, A.; Lazzarotto, E.; Markovitsi, D.; Scalmani, G.; Frisch, M. J.; Barone, V.; Improta, R. *J. Am. Chem. Soc.* **2006**, *128*, 607.
(16) Pecourt, J.-M. L.; Peon, J.; Kohler, B. J. *Am. Chem. Soc.* **2001**, *132*, 10370.
(17) Hare, P. M.; Crespo-Hernández, C. E.; Kohler, B. *Proc. Natl. Acad. Sci. U.S.A.* **2007**, *104*, 435.
(18) Gustavsson, T.; Bányász, A.; Sarkar, N.; Markovitsi, D.; Improta, R. *Chem. Phys.* **2008**, *350*, 186.
(19) Improta, R.; Barone, V.; Lami, A.; Santoro, F. *J. Phys. Chem. B* **2009**, *113*, 14491.
(20) Nakayama, A.; Arai, G.; Yamazaki, S.; Taketsugu, T. *J. Chem. Phys.* **2013**, *139*, 214304.
(21) Minezawa, N. *J. Chem. Phys.* **2014**, *141*, 164118.
(22) Urano, S.; Yang, X.; LeBreton, P. R. *J. Mol. Struct.* **1989**, *214*, 315.
(23) Buchner, F.; Lübcke, A.; Heine, N.; Schultz, T. *Rev. Sci. Instrum.* **2010**, *81*, 113107.
(24) Preissler, N.; Buchner, F.; Schultz, T.; Lübcke, A. *J. Phys. Chem. B* **2013**, *117*, 2422.
(25) Buchner, F.; Ritze, H.-H.; Lahl, J.; Lübcke, A. *Phys. Chem. Chem. Phys.* **2013**, *15*, 11402.
(26) Wu, Y.; Tepper, H. L.; Voth, G. A. *J. Chem. Phys.* **2006**, *124*, 024503.
(27) Werner, H. J., Knowles, P. J., Knizia, G., Manby, F. R., Celani, M. S. P., Korona, T., Lindh, R., Mitrushenkov, A., Rauhut, G., Shamasundar, K. R., Adler, T. B., Amos, R. D., Bernhardsson, A., Berning, A., Cooper, D. L., Deegan, M. J. O., Dobbyn, A. J., Eckert, F., Goll, E., Hampel, C., Hesselmann, A., Hetzer, G., Hrenar, T., Jansen, G., Köppl, C., Liu, Y., Lloyd, A. W., Mata, R. A., May, A. J., McNicholas, S. J., Meyer, W., Mura, M. E., Nicklaß, A., O'Neill, D. P., Palmieri, P., Pflüger, K., Pitzer, R., Reiher, M., Shiozaki, T., Stoll, H., Stone, A. J., Tarroni, R., Thorsteinsson, T., Wang, M., Wolf, A. *MOLPRO version 2010.1 a package of ab initio programs*; Birmingham, UK.
(28) Zechmann, G.; Barbatti, M. *J. Phys. Chem. A* **2008**, *112*, 8273.
(29) Etinski, M.; Marian, C. M. *Phys. Chem. Chem. Phys.* **2010**, *12*, 4915.
(30) Tao, H.; Levine, B. G.; Martínez, T. J. *J. Phys. Chem. A* **2009**, *113*, 13656.
(31) Schreiber, M.; Silva-Junior, M. R.; Sauer, S. P. A.; Thiel, W. *J. Chem. Phys.* **2008**, *128*, 134110.
(32) See the Supporting Information.
(33) Onidas, D.; Markovitsi, D.; Marguet, S.; Sharonov, A.; Gustavsson, T. *J. Phys. Chem. B* **2002**, *106*, 11367.
(34) Konovalov, V. V.; Raitsimring, A. M.; Tsvetkov, Y. D. *Int. J. Rad. Appl. Instr. C Rad. Phys. Chem.* **1988**, *32*, 623.
(35) Plante, I.; Cucinotta, F. A. *New J. Phys.* **2009**, *11*, 063047.
(36) Buchner, F.; Schultz, T.; Lübcke, A. *Phys. Chem. Chem. Phys.* **2012**, *14*, 5837.
(37) Suzuki, Y.-I.; Nishizawa, K.; Kurahashi, N.; Suzuki, T. *Phys. Rev. E* **2014**, *90*, 010302(R).
(38) Matsika, S. *J. Phys. Chem. A* **2005**, *109*, 7538.
(39) Kistler, K. A.; Matsika, S. *J. Chem. Phys.* **2008**, *128*, 215102.
(40) González-Vázquez, J.; González, L. *Chem. Phys. Chem.* **2010**, *11*, 3617.
(41) Satzger, H.; Townsend, D.; Zgierski, M. Z.; Patchkovskii, S.; Ullrich, S.; Stolow, A. *Proc. Natl. Acad. Sci. U.S.A.* **2006**, *103*, 10196.

DOI: 10.1021/ja511108u
J. Am. Chem. Soc. 2015, 137, 2931−2938